Hindawi
Geofluids
Volume 2021, Article ID 8879205, 10 pages
https://doi.org/10.1155/2021/8879205

Research Article

Modelling of Transient CO_2/Water Flow in Wellbore considering Multiple Mass and Heat Transfer

Xinxin Zhao,[1,2] **Xiangzhen Yan**,[1] **Xiaohui Sun**,[1,2] **Qing Zhao**,[3] **Hongwei Jiang**,[3] **Yonghai Gao**,[1,2] **and Guang Yang**[3]

[1]*Key Laboratory of Unconventional Oil & Gas Development (China University of Petroleum (East China)), Ministry of Education, Qingdao 266580, China*
[2]*School of Petroleum Engineering, China University of Petroleum (East China), Qingdao 266580, China*
[3]*CNPC Engineering Technology R & D Company Limited, Beijing 102206, China*

Correspondence should be addressed to Xiangzhen Yan; 871811196@qq.com

Received 8 September 2020; Revised 16 February 2021; Accepted 22 February 2021; Published 18 March 2021

Academic Editor: Guanglong Sheng

A transient fully coupled model is proposed to investigate the two-phase flow of CO_2 and water-based fluid in a wellbore, considering the complex mass and heat transfer in different flow patterns and dynamic coupling between the wellbore and reservoir. Based on mass conservation, momentum, and energy balance, the model employs a state-of-the-art equation of state and transport models to analyze the variations of multiphase flow behaviors and CO_2 properties in a wellbore. Applied in the scenario of a drilled gas kick, the proposed model is used to simulate the processes of gas migration and two-phase flow in the wellbore. The results indicate that the CO_2 solubility increases gradually with the increment of depth, the trend of which shows an abrupt change in 500-1000 m due to the phase transition of CO_2. During kick development, the fronts of free gas and dissolved gas increase almost linearly with time. Through a comparison of CO_2 and CH_4 kicks, gas dissolution is found to significantly suppress the development process of CO_2 kick. The error in kick prediction can reach 42% if the effect of gas dissolution is neglected. However, it can be neglected for CH_4 kick.

1. Introduction

As an important greenhouse gas, carbon dioxide has aroused wide concern in the field of energy and environment. Its use in energy development is one of the hot researches recently. Compared to the conventional working fluids, liquid or supercritical CO_2 has good properties (large density and heat capacity, low viscosity, and surface tension, etc.) for heat transfer and fluid flow and is widely used in the operations of drilling, fracturing, enhanced oil recovery (EOR), and geothermal exploitation [1–5]. Generally, affected by variations of the temperature and pressure in the wellbore, the thermophysical properties of CO_2 change significantly in the temporal and spatial scales, as shown in Figure 1. Particularly, there exist complicated flow patterns and mass and heat transfer processes while CO_2 and water-based fluid coexisting in the wellbore. Therefore, it is necessary to develop a reliable model for transient CO_2/water flow, which can be of important significance for accurate prediction and control of multiphase flow parameters in the actual wellbore/reservoir systems.

At present, a lot of research works have been done to model the single CO_2 flow in the wellbore during the processes of CO_2 drilling, injection, and production [6–8]. In actual operations, the wellbore two-phase flow of CO_2 and water can be generated due to the influx of formation fluids (such as a drilled gas kick). As the flow of different fluid components, the phase interface may exhibit various flow patterns, accompanied with complicated mass and heat transfer phenomena. Zha et al. [9] proposed an equivalent single-phase flow model to interpret the oil-water two-phase flow in a wellbore during the well test period. Shang et al. [10] developed a mathematical model coupling fluid flow in the horizontal wellbore and reservoir, based on the principle of mirror reflection and mass conservation. Regarding the nonisothermal multiphase flow

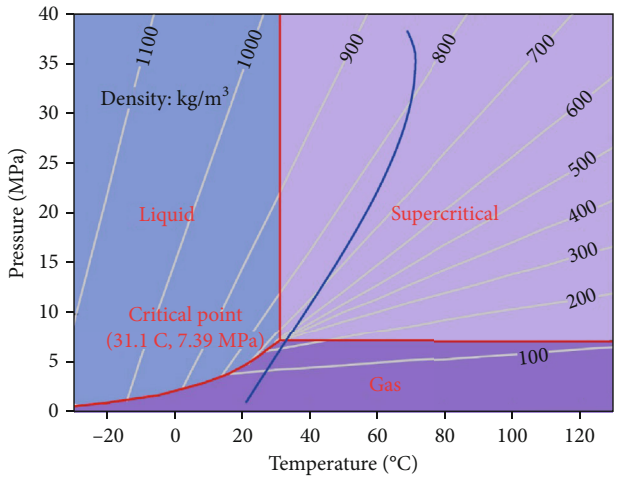

FIGURE 1: Phase diagram of carbon dioxide. The blue curve represents a typical temperature-pressure distribution in the wellbore as CO_2 flow. As seen, the phase and thermophysical properties of CO_2 can vary significantly.

process in the wellbore, Pan and Oldenburg [11] developed an integrated simulator based on the drift-flux model, which can be applied in the process of geothermal exploitation using supercritical CO_2. Considering the migration characteristics of gas kick in the wellbore, He et al. [12] built a kick simulation model and analyzed the effect of sour gas dissolution on well control operations. Lu and Connell [13] developed a quasi-steady wellbore two-phase flow model to simulate the non-isothermal flow of carbon dioxide in injection wells during geological storage. Recently, Wang et al. [14–16] proposed a series of calculation models of CO_2 density, friction coefficient, Joule–Thomson coefficient, and so on, which can significantly improve the simulation accuracy of CO_2 thermophysical parameters in the wellbore in the drilling scenario. Based on that, they developed the wellbore temperature and pressure models considering the phase transition of sour gases. These models can perform more accurate estimations of wellbore temperature and pressure fields [17–19]. Their simulation results indicated that the gas kicks can be "hidden" and "abrupt" successively, affected by the phase transition of the fluids in the dynamically changing temperature and pressure environment. Furthermore, the critical wellhead back pressures for suppressing the abrupt expansion of sour gases were obtained [20]. These research and findings can provide a solid theoretical basis for early kick detection and wellbore pressure control.

In this study, we developed a transient fully coupled model for wellbore CO_2/water flow, which considers the complicated mass and heat transfer mechanisms in different flow patterns and the dynamical coupling between wellbore and reservoir. Subsequently, the proposed model is applied to analyze the multiphase flow process during a drilled CO_2 kick.

2. Wellbore Multiphase Flow Model

2.1. Mass Conservation Equation. Considering the one-dimensional unsteady flow [19], the equations expressing the mass conservation laws among the free CO_2 phase, continuous water phase, and dissolved CO_2 phase can be presented as follows:

(1) Free CO_2 phase

$$\frac{\partial}{\partial t}\left(A\alpha_{CO2}\rho_{CO2}\right)+\frac{\partial}{\partial s}\left(A\alpha_{CO2}\rho_{CO2}v_{CO2}\right)=-\dot{m}_L+q_g, \quad (1)$$

where t is the time, s; s is the distance, m; A is the cross-sectional area, m^2; α_{CO2} is the void fraction of free CO_2 phase; ρ_{CO2} is the CO_2 density, kg/m^3; v_{CO2} is the velocity of free CO_2 phase, m/s; $\dot{m}_L$ is the mass transfer rate of CO_2 dissolution, kg/(m•s); and q_g is the mass transfer rate of CO_2 between the wellbore and reservoir, kg/(m•s). The rate of CO_2 influx from reservoir to wellbore is mainly dominated by the pressure underbalance and reservoir properties, which can be estimated using the model of Sun et al. [21].

(2) Continuous water phase

$$\frac{\partial}{\partial t}\left(A\alpha_l\rho_l\right)+\frac{\partial}{\partial s}\left(A\alpha_l\rho_l v_l\right)=\dot{m}_L, \quad (2)$$

where α_l is the void fraction of continuous water phase; ρ_l is the density of water, kg/m^3; and v_l is the velocity of water, m/s.

(3) Dissolved CO_2 phase

$$\frac{\partial}{\partial t}\left(A\alpha_l x_{sol}\rho_l\right)+\frac{\partial}{\partial s}\left(A\alpha_l x_{sol}\rho_l v_l\right)=\dot{m}_L, \quad (3)$$

where x_{sol} is the mass fraction of dissolved gas, kg/kg.

In equations (1)–(3), the relation for velocities of different phases can be described by the drift-flux model:

$$v_{CO2}=C_0 v_l+v_\infty, \quad (4)$$

where C_0 is distribution coefficient, dimensionless and v_∞ is the drift velocity of gas, m/s. Commonly, the distribution coefficient and drift velocity are closely related to the flow pattern, phase distributions, pipeline configuration, etc. Here, the slip relation developed by Bhagwat and Ghajar [22] is employed.

2.2. Momentum Conservation Equation.

$$\begin{aligned}&\frac{\partial}{\partial t}\left(A\alpha_{CO2}\rho_{CO2}v_{CO2}+A\alpha_l\rho_l v_l\right)\\&\quad+\frac{\partial}{\partial s}\left(A\alpha_{CO2}\rho_{CO2}v_{CO2}^2+A\alpha_l\rho_l v_l^2\right)\\&\quad+\frac{\partial}{\partial s}\left(Ap\right)=-Af\frac{\rho_m v_m^2}{2d_c}+A\rho_m g\cos\theta,\end{aligned} \quad (5)$$

where ρ_m is the density of fluid mixture, kg/m^3; v_m is the velocity of fluid mixture, m/s; p is pressure, Pa; d_c is the hydraulic diameter, m; θ is the inclination angle, rad; and g is gravitational acceleration, m/s^2. In equation (5), f is the

friction coefficient, which can be described using the model of Wang et al. [15].

$$\begin{cases} f = \dfrac{64}{\mathrm{Re}}, & \mathrm{Re} < 2300, \\ f = 0.06539 \times \exp\left(-\left(\dfrac{\mathrm{Re} - 3516}{1248}\right)^2\right), & 2300 \le \mathrm{Re} \le 3400, \\ \dfrac{1}{\sqrt{f}} = -2.34 \times \lg\left(\dfrac{\varepsilon}{1.72 d_c} - \dfrac{9.26}{\mathrm{Re}} \times \lg\left(\left(\dfrac{\varepsilon}{29.36 d_c}\right)^{0.95} + \left(\dfrac{18.35}{\mathrm{Re}}\right)^{1.108}\right)\right), & 3400 < \mathrm{Re} < 2 \times 10^6, \end{cases} \tag{6}$$

where Re is the Reynolds number, dimensionless and ε is roughness, m.

2.3. Energy Conservation Equation. Considering the phase transition, Joule–Thomson cooling, heat transfer between the wellbore and formations, and reservoir coupling, the temperature model for wellbore CO_2/water flow can be obtained based on energy conservation [23]:

$$\begin{aligned} & A\left(\alpha_{\mathrm{CO2}}\rho_{\mathrm{CO2}}C_{p,\mathrm{CO2}} + \alpha_l\rho_l C_{p,l}\right)\frac{\partial T}{\partial t} \\ & + A\left(\alpha_{\mathrm{CO2}}\rho_{\mathrm{CO2}}C_{p,\mathrm{CO2}}v_{\mathrm{CO2}} + \alpha_l\rho_l C_{p,l}v_l\right)\frac{\partial T}{\partial s} \\ & - A\alpha_{\mathrm{CO2}}\rho_{\mathrm{CO2}}C_{p,\mathrm{CO2}}C_J\frac{\partial p}{\partial t} \\ & + \frac{1}{2}\frac{\partial}{\partial t}\left[A\left(\alpha_{\mathrm{CO2}}\rho_{\mathrm{CO2}}v_{\mathrm{CO2}}^2 + \alpha_l\rho_l v_l^2\right)\right] \\ & + \frac{1}{2}\frac{\partial}{\partial s}\left[A\left(\alpha_{\mathrm{CO2}}\rho_{\mathrm{CO2}}v_{\mathrm{CO2}}^3 + \alpha_l\rho_l v_l^3\right)\right] \\ & - A\alpha_{\mathrm{CO2}}\rho_{\mathrm{CO2}}C_{p,\mathrm{CO2}}v_{\mathrm{CO2}}C_J\frac{\partial p}{\partial s} \\ & - \frac{\partial(Ap)}{\partial t} = -A(\alpha_{\mathrm{CO2}}\rho_{\mathrm{CO2}}v_{\mathrm{CO2}} \\ & + \alpha_l\rho_l v_l)g\cos\theta + q_g\left(h_e - h_g\right) + Q_{\mathrm{transfer}} \\ & + Af\frac{\rho_m v_m^3}{2d_c} + \dot{m}_L\Delta H_{\mathrm{sol}}, \end{aligned} \tag{7}$$

where T is the fluid temperature, ˚C; $C_{p,\mathrm{CO2}}$ is specific heat capacity of CO_2 at constant pressure, J/(kg•˚C); $C_{p,l}$ is specific heat capacity of the liquid phase at constant pressure, J/(kg•˚C); C_J is the Joule–Thomson coefficient of gas, ˚C/Pa; h_e is the enthalpy of the influx gas at reservoir condition, J/kg; h_g is the enthalpy of CO_2 in the wellbore, J/kg; ΔH_{sol} is the dissolution heat of gas in water, J/kg; Q_{transfer} is the rate of heat exchange between the wellbore and formations, $Q_{\mathrm{transfer}} = Q(h, \Delta T, r_i, \lambda_i, t)$; h is the convective heat transfer coefficient, W/(m^2•˚C); ΔT is the temperature difference, ˚C; r_i represents the geometric size of wellbore system, m; and λ_i is the thermal conductivity of wellbore system, W/(m•˚C).

Generally, the Joule–Thomson effect of water can be negligible compared to that of CO_2. According to the PVT properties of gas, the Joule–Thomson coefficient of CO_2 is defined as follows:

$$\mu_{JT} = \lim_{\Delta P \to 0}\left(\frac{\Delta T}{\Delta P}\right)_H = \left(\frac{\partial T}{\partial P}\right)_H. \tag{8}$$

Wang et al. [16] revealed that the absolute average errors of the CO_2 Joule–Thomson coefficient predicted by the state equations are relatively low in vapor and supercritical states, but larger errors appear near the CO_2 critical point and liquid state. Therefore, they built a religious empirical model, in which the absolute average errors at the vapor, liquid, and supercritical states are 1.52%, 4.59%, and 3.08%, respectively.

$$\begin{aligned} C_J = {} & \frac{(\eta - \eta_1)(\eta - \eta_2)(1 - \eta)}{\eta_1\eta_2}\mu_{\mathrm{JT}-(0)} \\ & + \frac{\eta(\eta - \eta_2)(\eta - 1)}{\eta_1(\eta_1 - \eta_2)(\eta_1 - 1)}\mu_{\mathrm{JT}-(1)} \\ & + \frac{\eta(\eta - \eta_1)(\eta - 1)}{\eta_2(\eta_2 - \eta_1)(\eta_2 - 1)}\mu_{\mathrm{JT}-(2)} \\ & + \frac{\eta(\eta - \eta_1)(\eta - \eta_2)}{(\eta_1 - 1)(\eta_2 - 1)}, \end{aligned} \tag{9}$$

where $\eta, \eta_1, \eta_2, \mu_{\mathrm{JT}-(0)}, \mu_{\mathrm{JT}-(1)}$, and $\mu_{\mathrm{JT}-(2)}$ are the functions of temperature and pressure.

3. Mass and Heat Transfer for Different Flow Patterns

3.1. Flow Pattern Transition. The mass and heat transfer characteristics in the two-phase flow are significantly governed by the flow patterns. In this study, the model developed by Hasan and Kabir [24] is used to flow pattern identification, as shown in Table 1.

3.2. Interphase Mass Transfer Model. The dissolution of sour gas in the wellbore two-phase flow is a diffusion process governed by concentration difference. Therefore, the gas dissolution rate is a function of gas concentration and mass transfer

Table 1: Criteria of gas/liquid flow pattern transition.

Flow pattern	Criteria
Bubble flow	$v_{gs} > (0.429v_{Ls} + 0.357v_{\infty})\cos\theta$ or $\alpha_g < 0.52$, and $v_m^{1.12} > 4.68d_c^{0.48}\left[g\left(\rho_L - \rho_g\right)/\sigma\right]^{0.5}(\sigma/\rho_L)^{0.6}(\rho_m/\mu_L)^{0.08}$
Slug flow	$v_{gs} > (0.429v_{Ls} + 0.357v_{\infty})\cos\theta$ and $v_{gs}^2\rho_g < \left[17.1\log_{10}\left(v_{Ls}^2\rho_L\right) - 23.2\right]$ if $v_{Ls}^2\rho_L < 50v_{gs}^2\rho_g < 0.00673\left(v_{Ls}^2\rho_L\right)^{1.7}$ if $v_{Ls}^2\rho_L \geq 50$
Churn flow	$v_{gs} < 3.1\left[\sigma g\left(\rho_L - \rho_g\right)/\rho_g^2\right]^{0.25}$ and $v_{gs}^2\rho_g < \left[17.1\log_{10}\left(v_{Ls}^2\rho_L\right) - 23.2\right]$ if $v_{Ls}^2\rho_L < 50v_{gs}^2\rho_g < 0.00673\left(v_{Ls}^2\rho_L\right)^{1.7}$ if $v_{Ls}^2\rho_L \geq 50$
Annular flow	$v_{gs} > 3.1\left[\sigma g\left(\rho_L - \rho_g\right)/\rho_g^2\right]^{0.25}$

Note that v_{gs} is the superficial velocity of gas phase, m/s and v_{Ls} is the superficial velocity of liquid phase, m/s.

Table 2: Main parameters of the kicking well.

Parameter	Value	Parameter	Value
Well depth	3718.84 m	Displacement	30 L/s
Density of drilling fluid	1.43 g/cm^3	Plastic viscosity	30 mPa•s
Yield value	15 Pa	Permeability	480 mD
Geothermal gradient	1.9°C/100 m	Surface temperature	26°C
Shut-in standpipe pressure	1.9 MPa	Shut-in casing pressure	2.0 MPa
Wellbore configuration: 20″ casing × 70 m + 17 − 1/2″ casing × 900 m + φ 320 mm open hole × 3718.84 m			
Drilling assembly: EH1317φ319 mm PDC × 0.41 m + 8″ drill collar × 80m + 5″ heavy weight drill pipe × 120.53 m + 5″ drill pipe × 1392.56 m + 5 − 1/2″ drill pipe			

coefficient:

$$\dot{m}_L = M_g S_{\text{int}} k_M (c_{\text{sat}} - c), \tag{10}$$

where c is the gas concentration, mol/m^3; c_{sat} is the gas concentration at saturation, mol/m^3; M_g is the molecular mass of CO_2, kg/mol; k_M is the interphase mass transfer coefficient between CO_2 and liquid phase, m/s; and S_{int} is the contact area of CO_2 and liquid phase, m^2. In this study, the contact area in different flow patterns is estimated using the model proposed by Sun et al. [23].

The determination of the mass transfer coefficient, which is related to the fluid properties (such as density, viscosity, and diffusivity), flow velocity, and annulus size, is challenging. Considering the laminar flow and turbulent flow conditions, the expression presented by Cussler [25] is employed.

$$k_M = \begin{cases} 1.62\dfrac{D_g}{d_c}\left(\dfrac{d_c^2 v_{\text{CO2}}}{LD_g}\right)^{1/3}, & \text{Laminar flow,} \\ 0.026\dfrac{D_g}{d_c}\left(\dfrac{d_c v_{\text{CO2}}}{\upsilon}\right)^{0.8}\left(\dfrac{\upsilon}{D_g}\right)^{1/3}, & \text{Turbulent flow,} \end{cases} \tag{11}$$

where L is the pipe length, m; ν is the kinematic viscosity, m^2/s; and D_g is the gas diffusivity coefficient, m^2/s.

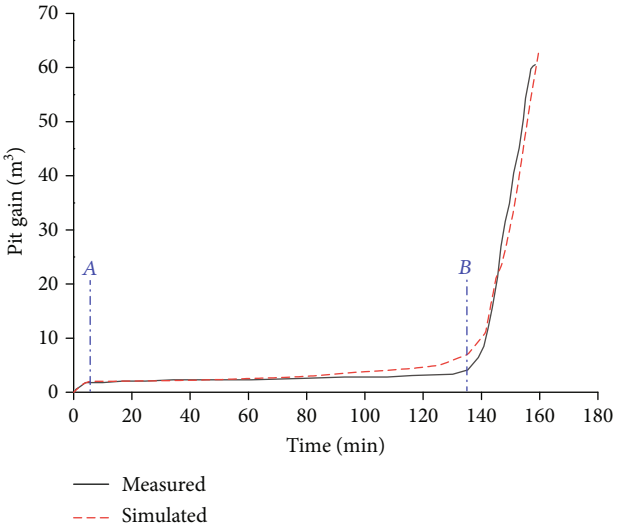

Figure 2: Comparison between measured and simulated pit gains during CO_2 kick.

Furthermore, we use the model of Duan and Sun [26] to calculate the CO_2 solubility in water-based fluid in this study.

$$\ln\frac{y_{\text{CO}_2}P\rho_l}{c_{\text{sat}}} = \frac{\mu_{\text{CO}_2}^{\text{l}(0)}}{RT} - \ln\varphi_{\text{CO}_2} + \sum_c 2\lambda_{\text{CO}_2-c}m_c + \sum_a 2\lambda_{\text{CO}_2-a}m_a + \sum_c\sum_a \zeta_{\text{CO}_2-c-a}m_c m_a, \tag{12}$$

where φ_{CO2} is the fugacity coefficient of CO_2 and y_{CO2} is the

Table 3: Basic parameters for kick simulation.

Parameter	Value	Parameter	Value
Well type	Vertical	Well depth	3500 m
Reservoir temperature	125°C	Reservoir pressure	42 MPa
Rock permeability	50 mD	Porosity	0.15
Temperature gradient	0.03°C/m	Total compressibility	0.0002 (1/MPa)
Density of drilling fluid	1050 kg/m^3	Displacement	0.02 m^3/s
Surface temperature	20°C	Viscosity of drilling fluid	20 cp
Rate of penetration	10 m/h	Simulation time	500 s

mole fraction of CO_2 in vapor phase, λ_{CO2-c} is the binary interaction parameter of CO_2 and cation, λ_{CO2-a} is the binary interaction parameter of CO_2 and anion, and $\zeta_{CO2-c-a}$ is the ternary interaction parameter of CO_2, cation, and anion.

3.3. Convection Heat Transfer Model in Different Flow Patterns. As wellbore multiphase flow, convection heat transfer mainly occurs in the heat transfer boundary layer. Therefore, the flow pattern can have an important influence on the heat transfer mechanisms. Generally, the convection heat transfer coefficient can be written as follows:

$$h = \frac{\mathrm{Nu}\lambda}{d_c}, \tag{13}$$

where λ is the thermal conductivity of CO_2, W/(m•°C).

Through the experiments of heat transfer in wellbore multiphase flow, Gao et al. [27] proposed the model of convection heat transfer coefficient in different flow patterns.

$$\mathrm{Nu} = a\,\mathrm{Re}^{0.7922}\,\mathrm{Pr}^{0.3}\left(\frac{\mu_f}{\mu_w}\right)^{0.25}\left(1 - b\alpha_g^c\right), \tag{14}$$

where Pr is the Prandtl number, μ_f is the fluid viscosity at characteristic temperature, Pa•s; μ_w is the fluid viscosity at surface temperature, Pa•s; a, b, and c are constants related to flow patterns: $a = 0.01215$, $b = 0.30577$, and $c = -0.16578$ for bubble flow; $a = 0.46359$, $b = 0.97599$, and $c = -0.01314$ for slug flow; and $a = 0.50861$, $b = 0.93808$, and $c = -0.15418$ for churn flow and annular flow.

Furthermore, the thermophysical properties of CO_2 vary greatly accompanied with the complicated mass and heat transfer processes. The detailed calculation models for thermophysical parameters of CO_2 are presented in Appendix A.

4. Model Simulation and Verification

4.1. Model Simulation. The integrated model is solved using the simulation method proposed by Sun et al. [23], which employs a fully implicit scheme, constant space steps, and varying time steps. The overall simulation process is consisting of three layers of iterations. At first, the phase velocities and fractions at different space blocks are calculated based on a drift-flux model. Subsequently, the pressure field is estimated using a predictor-corrector shooting technique. With updating the fluid properties and multiphase flow parameters, the temperature distribution in the drilling pipe and annulus are iteratively simulated until a desired convergence tolerance is achieved.

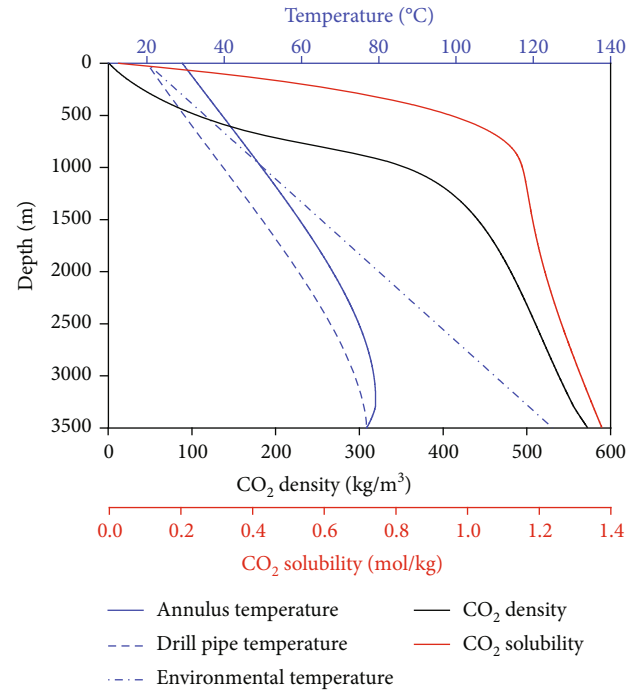

Figure 3: The distribution of fluid temperature and CO_2 density and solubility in the wellbore at 500 s.

4.2. Model Verification. The proposed model is validated using the measured data of a field well, which comes across a CO_2 kick accident. The pit gain approaches 1.9m^3 at 12:00 when the alarm sounded. Then, the well was shut to measure the standpipe pressure and casing pressure. At 13:05, the gas influx was circulated gradually while a constant casing pressure (2 MPa) is maintained. At 15:30, a large amount of CO_2 blows out from the wellhead. The main parameters of the kicking well are presented in Table 2.

Figure 2 shows the simulated and measured pit gains during CO_2 kick. At point A, the gas kick was detected with a pit gain of 1.9 m^3. The multiphase flow process of gas circulation is simulated from point A to point B, in which the pressure underbalance and gas influx rate at the bottom hole is low. CO_2 dissolves into the drilling fluid gradually, which leads to the nonobvious variations in pit gain. After point B, the

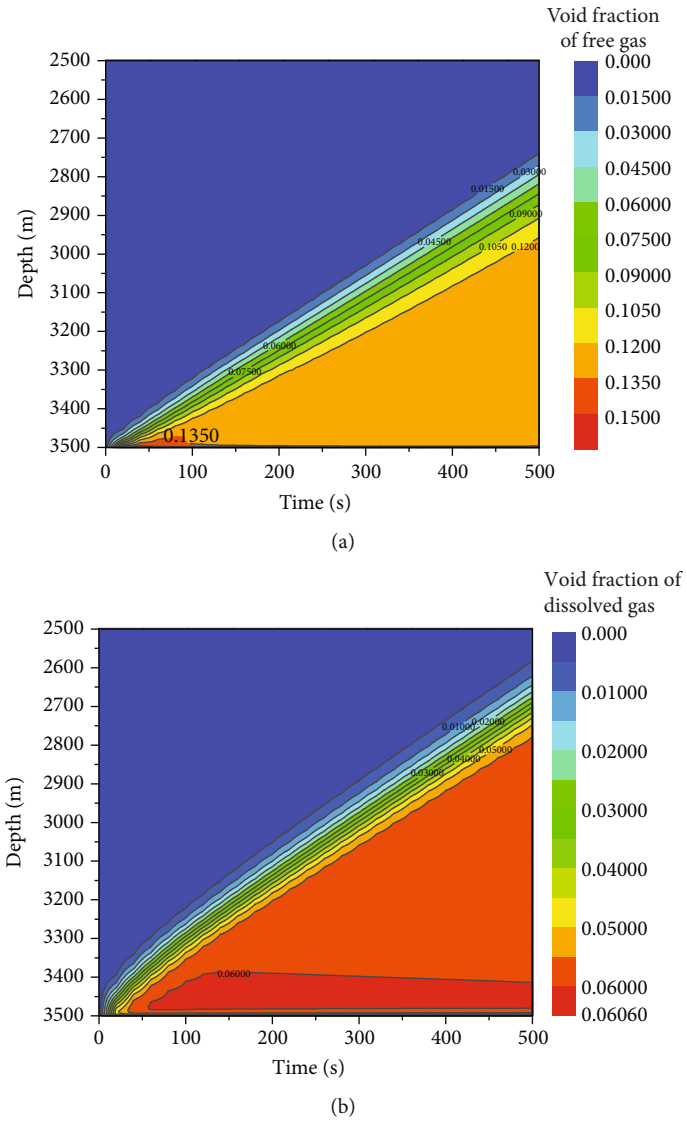

Figure 4: (a) The distribution of free gas in the wellbore at different times. (b) The distribution of dissolved gas in the wellbore at different times.

dissolved CO_2 rapidly releases out from the drilling fluid due to the decrease of gas solubility near the surface.

As seen, the simulated results of pit gain agree well with the measured data, and the average error is 3.253%. It indicates that the proposed model can accurately describe the effect of phase transition on gas migration in wellbore.

5. Case Analysis

The formation fluids can enter the wellbore driven by pressure underbalance, if the bottom hole pressure at open hole section is less than the pore pressure during drilling. The understanding of phase transition and kick migration is important for early kick detection and wellbore control procedure. Using the proposed model, we simulate and analyze the flow behaviors of CO_2 and water-based fluid in the scenario of a drilled CO_2 kick. The basic parameters for kick simulation [19] are shown in Table 3.

5.1. Analysis of the Gas Migration Process. Figure 3 shows the profiles of fluid temperature and CO_2 density and solubility in the wellbore at 500 s. As seen, the wellbore temperatures increase gradually with the well depth increasing, affected by variations of the formation temperatures. At a given depth, the fluid temperature in the annulus is larger than that in the drill pipe.

Due to the dynamically changing temperature and pressure fields, the thermophysical properties of CO_2 vary significantly along the wellbore. Furthermore, the variation trend can be abrupt at 500 m to 1000 m because of phase transition. There results indicate that the free gas and dissolved gas can rapidly expand and separate out, respectively, which will pose a challenge to kick management and well control.

Figures 4(a) and 4(b) show the dynamical distributions of the free gas and dissolved gas in the wellbore at different times. As shown in Figure 4, the volume of gas influx in the wellbore increases gradually with time. And the front of gas

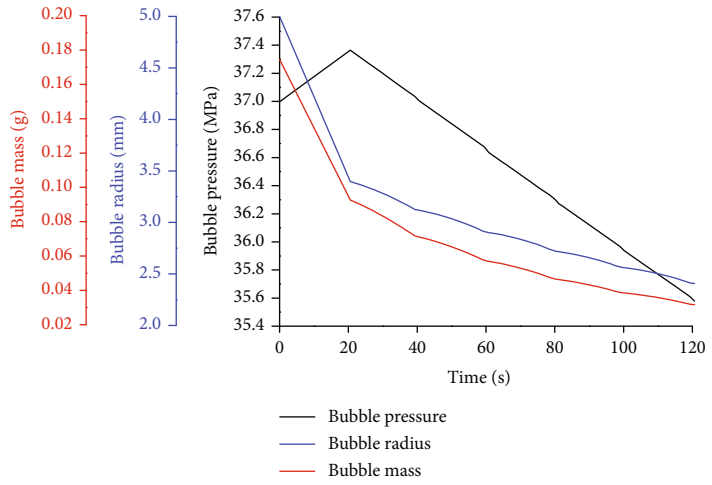

Figure 5: Variations of the pressure, radius, and mass of a gas bubble released at the initial time of gas kick (initial radius: 5 mm).

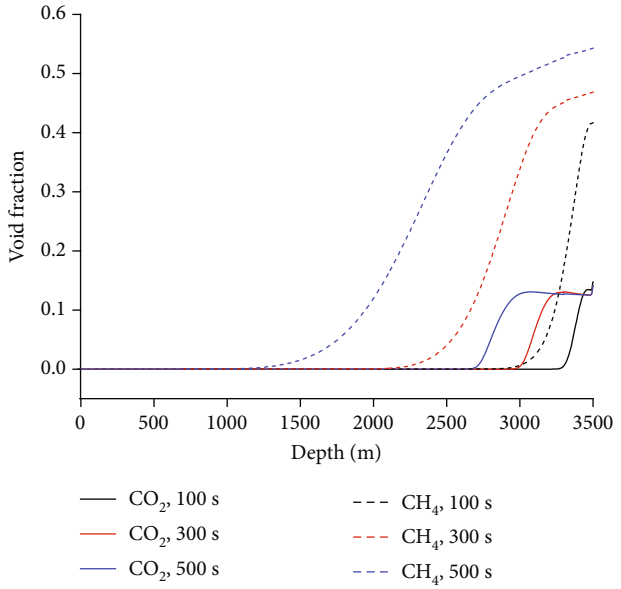

Figure 6: The profiles of free gas along the wellbore during methane and CO_2 kicks.

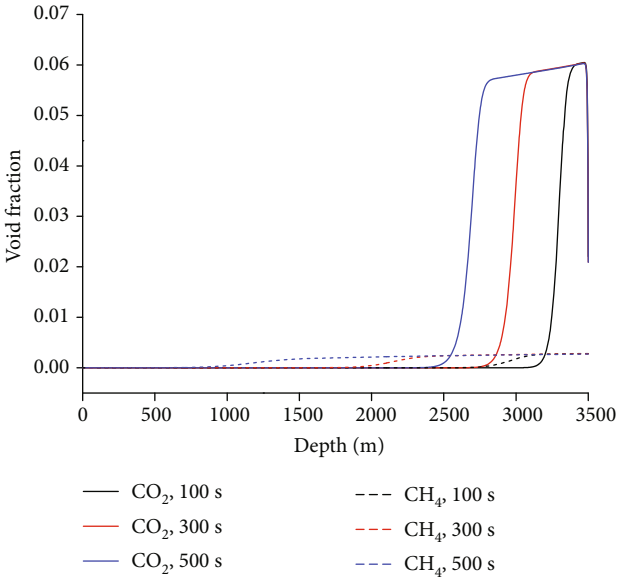

Figure 7: The profiles of dissolved gas along the wellbore during methane and CO_2 kicks.

profiles rises nearly linearly with time. In general, the void fraction of free gas increases as the increment of well depth.

As shown in Figure 4, the gas dissolves into the drilling fluids gradually as it migrates upward in the wellbore. The void fraction of dissolved gas reaches saturation state with time increasing, which can be a dynamical process. For example, the void fraction of dissolved gas at 3400 m increases rapidly at first and then decreases slightly due to variation of the gas solubility. It can be expected that the gas dissolution process will significantly suppress the migration and expansion of gas kick in the wellbore. After the gas kick initializes 500 s, the void fraction of dissolved gas is 42 percent of that of free gas near the bottom hole.

In this section, we study the migration process of a gas bubble which is released at the bottom hole as the gas kick initializes, as shown in Figure 5.

The gas influx rate at the open hole section is mainly governed by the wellbore pressure distribution, which consists of hydrostatic pressure and friction pressure. As the gas kick enters the wellbore, the flow velocity and friction pressure of fluid mixture will increase abruptly, which can lead to the sudden increment of bottom hole pressure. Subsequently, the decrease of hydrostatic pressure plays a dominant role, and the bubble pressure decreases gradually.

As seen, the bubble radius and mass decrease gradually with time. However, the bubble shrinkage rate decreases gradually due to the decrease of gas/liquid contact area and mass transfer rate. Furthermore, the volume change of gas bubble is also affected by the pressure change. At the early stage, the increment of bubble pressure will increase the bubble shrinkage rate. Then the decrease of bubble pressure will decrease the rate of bubble shrinkage.

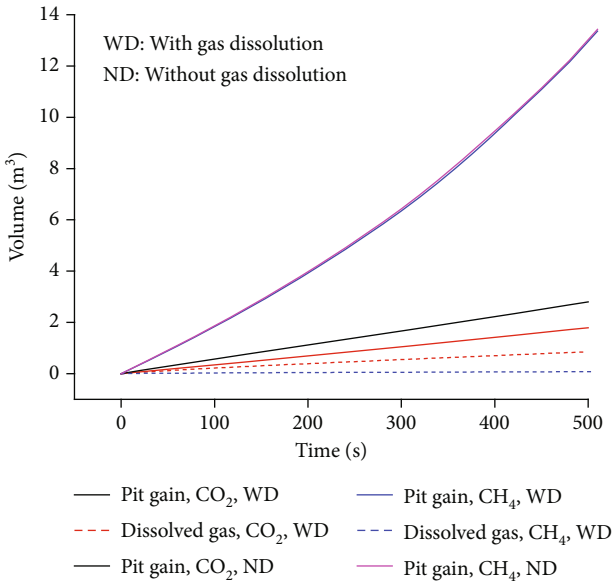

Figure 8: Comparison of the pit gain at different times during methane and CO_2 kicks.

5.2. Effect of Gas Dissolution. A comparison of CO_2 and CH_4 kicks is conducted to analyze the effect of gas dissolution and phase transition on kick migration.

Figure 6 shows the distributions of free gas along the wellbore during methane and CO_2 kicks. For a given depth, the void fraction of methane is significantly larger than that of CO_2. Because the gas influx rate for methane kick is larger under the same pressure underbalance, since the viscosity and percolation resistance of methane in reservoir are much smaller than that of CO_2. Affected by the large gas influx rate, the velocity of the fluid mixture is larger and gas front rises faster during the methane kick.

Figure 7 shows the distributions of dissolved gas along the wellbore during methane and CO_2 kicks. Under the same temperature and pressure condition, the solubility of carbon dioxide in water is much larger than that of methane. At 3000 m, we find that the void fraction of dissolved CO_2 is 20 times larger than that of dissolved methane.

As shown in Figure 8, the effect of gas dissolution on kick migration can be negligible in the methane kick, because the solubility of methane in water is low. As for the CO_2 kick, it can be found that gas dissolution has an important influence on the process of kick development. In the figure, the simulation error of pit gain can reach 50% if the effect of gas dissolution is neglected at 500 s.

6. Conclusions

(1) A transient fully coupled model for the two-phase flow of CO_2 and water-based fluid in wellbore is developed, considering the mass and heat transfer in different flow patterns and the dynamic coupling between wellbore and reservoir. Model validation against the measured data of a kicking well indicates that it can produce an average error of 3.253%

(2) Affected by variations of the wellbore temperature and pressure fields, the solubility of CO_2 increases with depth, which shows an abrupt increasing trend at 500 m to 1000 m due to phase transitions

(3) A methane kick can develop more rapidly than a CO_2 kick, i.e., the velocity of gas migration and void fraction of gas in a methane kick are much larger

(4) The simulation error of pit gain can reach 50% if the effect of gas dissolution is neglected in the CO_2 kick. However, it is negligible in the methane kick

Appendix

A. Appendix: Calculation Models for the Thermophysical Parameters of CO_2

At different temperature and pressure conditions, the PVT relation of gas can be described using the PR equation:

$$P = \frac{RT}{V-b} - \frac{a}{V(V+b)+b(V-b)}. \tag{A.1}$$

The relation of enthalpies at different states can be written as follows:

$$H_2 - H_1 = \int_{V_1}^{V_2} \left[T\left(\frac{\partial P}{\partial T}\right)_V - P \right] dV + (PV)_2 - (PV)_1. \tag{A.2}$$

By substituting equation (A.2) into equation (A.1), we obtain

$$H = RT(Z-1) - \frac{\sqrt{2}a}{4b}\left[1 + \frac{\kappa T}{\sqrt{\alpha T T_c}}\right] \ln\left(\frac{Z + \left(1+\sqrt{2}\right)B}{Z + \left(1-\sqrt{2}\right)B}\right) + H_{\text{ideal}}, \tag{A.3}$$

where R is the gas constant; b, α, and κ are parameters in the PR equation, $a = a\,(b, \alpha, \kappa)$, $B = bP/RT$, and Z is the gas compression factor:

$$Z^3 - (1-B)Z^2 + \left(A - 2B - 3B^2\right)Z - \left(AB - B^2 - B^3\right) = 0, \tag{A.4}$$

where $A = ap/(RT)^2$.

According to the S-W model [28], the enthalpy of ideal gas is

$$H_{\text{ideal}} = RT\left(1 + \tau \times \phi^0\right), \tag{A.5}$$

where τ is the reduced temperature, $\tau = T_c/T$; ϕ^0 is the Helmholtz free energy of ideal gas.

Combining equations (A.3) and (A.5), the specific enthalpy of carbon dioxide can be obtained:

$$h_c = \frac{1}{M_g}\left(Z + \frac{T_c}{T}\phi^0\right) - \frac{\sqrt{2}a}{4bM_c}\left[1 + \frac{\kappa T}{\sqrt{\alpha T T_c}}\right]\ln \cdot \left(\frac{Z + \left(1+\sqrt{2}\right)B}{Z + \left(1-\sqrt{2}\right)B}\right),$$

$$C_p = \left(\frac{\partial h}{\partial T}\right)_P = \frac{d^2a}{dT^2} \times \frac{T}{2\sqrt{2}bM_c} \times \ln\left(\frac{Z + \left(1+\sqrt{2}\right)B}{Z + \left(1-\sqrt{2}\right)B}\right) + \frac{R(M-N)^2 M_c^{-1}}{M^2 - 2A(Z+B)} - \frac{R}{M_c} + \frac{C_{p,\text{ideal}}}{M_c}. \quad (A.6)$$

In which, the parameters are defined as follows:

$$M = \frac{\left(Z^2 + 2 \times B \times Z - B^2\right)}{(Z-B)}, \qquad N = \frac{(\mathrm{d}a/\mathrm{d}T)}{(B/bR)}. \quad (A.7)$$

Additionally, the viscosity and thermal conductivity of CO_2 can be estimated using the model of Vesovic et al. [29].

Nomenclature

Variables

A: Cross-sectional area (m^2)
C_0: Distribution coefficient, dimensionless
$C_{p,CO2}$: Specific heat capacity at constant pressure of CO_2 (J/(kg•°C))
$C_{p,l}$: Specific heat capacity at constant pressure of the liquid phase (J/(kg•°C))
C_J: Joule–Thomson coefficient of gas (°C/Pa)
c: Gas concentration (mol/m^3)
c_{sat}: Gas concentration at saturation (mol/m^3)
d_c: Hydraulic diameter (m)
D_g: Gas diffusivity coefficient (m^2/s)
f: Friction coefficient
g: Gravitational acceleration (m/s^2)
h_e: Enthalpy of the influx gas at reservoir condition (J/kg)
h_g: Enthalpy of CO_2 in the wellbore (J/kg)
ΔH_{sol}: Dissolution heat of gas in water (J/kg)
h: Convective heat transfer coefficient (W/(m^2•°C))
k_M: Interphase mass transfer coefficient between CO_2 and liquid phase (m/s)
L: Pipe length (m)
$\dot{m}_L$: Mass transfer rate of CO_2 dissolution (kg/(m•s))
M_g: Molecular mass of CO_2 (kg/mol)
p: Pressure (Pa)
Pr: Prandtl number
q_g: Mass transfer rate of CO_2 between the wellbore and reservoir (kg/(m•s))
$Q_{transfer}$: Rate of heat exchange between the wellbore and formations
R: Gas constant
Re: Reynolds number, dimensionless
r_i: Geometric size of wellbore system (m)
s: Distance (m)
S_{int}: Contact area of CO_2 and liquid phase (m^2)
T: Fluid temperature (°C)
t: Time (s)
ΔT: Temperature difference (°C)
v_{CO2}: Velocity of free CO_2 phase (m/s)
v_∞: Drift velocity of gas (m/s)
v_l: Velocity of water (m/s)
v_m: Velocity of fluid mixture (m/s)
v_{gs}: Superficial velocity of gas phase (m/s)
v_{Ls}: Superficial velocity of liquid phase (m/s)
x_{sol}: Mass fraction of dissolved gas (kg/kg)
y_{CO2}: Mole fraction of CO_2 in vapor phase.

Greek letters

α_{CO2}: Void fraction of free CO_2 phase
α_l: Void fraction of continuous water phase
ρ_{CO2}: CO_2 density (kg/m^3)
ρ_l: Density of water (kg/m^3)
ρ_m: Density of fluid mixture (kg/m^3)
θ: Inclination angle (rad)
ε: Roughness (m)
λ: Thermal conductivity of CO_2 (W/(m•°C))
λ_i: Thermal conductivity of wellbore system (W/(m•°C))
ν: Kinematic viscosity (m^2/s)
φ_{CO2}: Fugacity coefficient of CO_2
μ_f: Fluid viscosity at characteristic temperature (Pa•s)
μ_w: Fluid viscosity at surface temperature (Pa•s).

Data Availability

The data in this paper used to support the findings of this study are currently under embargo while the research findings are commercialized. Requests for data, 6 months after publication of this article, will be considered by the corresponding author.

Conflicts of Interest

The authors declare that they have no conflicts of interest.

References

[1] H. Singh, "Impact of four different CO_2 injection schemes on extent of reservoir pressure and saturation," *Advances in Geo-Energy Research*, vol. 2, no. 3, pp. 305–318, 2018.

[2] J. Zhou, N. Hu, X. Xian et al., "Supercritical CO_2 fracking for enhanced shale gas recovery and CO_2 sequestration: results,

status and future challenges," *Advances in Geo-Energy Research*, vol. 3, no. 2, pp. 207–224, 2019.

[3] G. Sheng, Y. Su, H. Zhao, and J. Liu, "A unified apparent porosity/permeability model of organic porous media: coupling complex pore structure and multi-migration mechanism," *Advances in Geo-Energy Research*, vol. 4, no. 2, pp. 115–125, 2020.

[4] R. Ershadnia, C. D. Wallace, and M. R. Soltanian, "CO_2 geological sequestration in heterogeneous binary media: effects of geological and operational conditions," *Advances in Geo-Energy Research*, vol. 4, no. 4, pp. 392–405, 2020.

[5] H. Liu, Z. Zhu, W. Patrick, J. Liu, H. Lei, and L. Zhang, "numerical visualization of supercritical CO_2 displacement in pore-scale porous and fractured media saturated with water," *Advances in Geo-Energy Research*, vol. 4, no. 4, pp. 419–434, 2020.

[6] F. A. Al-Adwani, J. Langlinais, and R. G. Hughes, "Modeling of an underbalanced-drilling operation using supercritical carbon dioxide," *SPE Drilling & Completion*, vol. 24, no. 4, pp. 599–610, 2009.

[7] X. Li, G. Li, H. Wang et al., "A unified model for wellbore flow and heat transfer in pure CO_2 injection for geological sequestration, EOR and fracturing operations," *International Journal of Greenhouse Gas Control*, vol. 57, pp. 102–115, 2017.

[8] B. Ruan, R. Xu, L. Wei, X. Ouyang, F. Luo, and P. Jiang, "Flow and thermal modeling of CO_2 in injection well during geological sequestration," *International Journal of Greenhouse Gas Control*, vol. 19, pp. 271–280, 2013.

[9] W. Zha, D. Li, Z. Lu, and B. Jia, "An equivalent single-phase flow for oil-water two-phase flow and its potential application in well test," *Advances in Geo-Energy Research*, vol. 2, no. 2, pp. 218–227, 2018.

[10] B. Shang, X. Han, S. Li, and K. Liu, "Research of water control technology for horizontal wells in water-driven reservoirs," *Advances in Geo-Energy Research*, vol. 2, no. 2, pp. 210–217, 2018.

[11] L. Pan and C. M. Oldenburg, "T2Well–An integrated wellbore-reservoir simulator," *Computers & Geosciences*, vol. 65, pp. 46–55, 2014.

[12] M. He, G. Liu, J. Li et al., "Study of sour gas kicks taken during managed pressure drilling operations," in *Paper SPE 176337-MS presented at SPE/IATMI Asia Pacific Oil & Gas Conference and Exhibition*, Nusa Dua, Bali, Indonesia, 2015.

[13] M. Lu and L. D. Connell, "Non-isothermal flow of carbon dioxide in injection wells during geological storage," *International Journal of Greenhouse Gas Control*, vol. 2, no. 2, pp. 248–258, 2008.

[14] Z. Wang, B. Sun, and L. Yan, "Improved density correlation for supercritical CO_2," *Chemical Engineering & Technology*, vol. 38, no. 1, pp. 75–84, 2015.

[15] Z. Wang, B. Sun, J. Wang, and L. Hou, "Experimental study on the friction coefficient of supercritical carbon dioxide in pipes," *International Journal of Greenhouse Gas Control*, vol. 25, no. 6, pp. 151–161, 2014.

[16] J. Wang, Z. Wang, and B. Sun, "Improved equation of CO_2 Joule-Thomson coefficient," *Journal of CO_2 Utilization*, vol. 19, pp. 296–307, 2017.

[17] Z. Wang, B. Sun, and X. Sun, "Calculation of temperature in fracture for carbon dioxide fracturing," *SPE Journal*, vol. 21, no. 5, pp. 1–10, 2016.

[18] Z. Wang, B. Sun, X. Sun, H. Li, and J. Wang, "Phase state variations for supercritical carbon dioxide drilling," *Greenhouse Gases: Science and Technology*, vol. 6, no. 1, pp. 83–93, 2016.

[19] X. Sun, Z. Wang, B. Sun, and W. Wang, "Research on hydrate formation rules in the formations for liquid CO_2 fracturing," *Journal of Natural Gas Science & Engineering*, vol. 33, pp. 1390–1401, 2016.

[20] B. Sun, P. Gong, and Z. Wang, "Simulation of gas kick with high H_2S content in deep well," *Journal of Hydrodynamics*, vol. 25, no. 2, pp. 264–273, 2013.

[21] J. Zhang, D. Du, and J. Hou, *Petrol-Gas Permeation Fluid Mechanics*, China University of Petroleum Press, Dong Ying, China, 2nd edition, 2010.

[22] S. M. Bhagwat and A. J. Ghajar, "A flow pattern independent drift flux model based void fraction correlation for a wide range of gas-liquid two phase flow," *International Journal of Multiphase Flow*, vol. 59, pp. 186–205, 2014.

[23] B. Sun, X. Sun, Z. Wang, and Y. Chen, "Effects of phase transition on gas kick migration in deepwater horizontal drilling," *Journal of Natural Gas Science and Engineering*, vol. 46, pp. 710–729, 2017.

[24] A. R. Hasan and C. S. Kabir, "Predicting multiphase flow behavior in a deviated well," *SPE Production Engineering*, vol. 3, no. 4, pp. 474–482, 1988.

[25] E. L. Cussler, *Diffusion: Mass Transfer in Fluid Systems*, Cambridge university press, New York, 2009.

[26] Z. Duan and R. Sun, "An improved model calculating CO_2 solubility in pure water and aqueous NaCl solutions from 273 to 533 K and from 0 to 2000 bar," *Chemical Geology*, vol. 193, no. 3-4, pp. 257–271, 2003.

[27] Y. Gao, Y. Cui, B. Xu et al., "Two phase flow heat transfer analysis at different flow patterns in the wellbore," *Applied Thermal Engineering*, vol. 117, pp. 544–552, 2017.

[28] R. Span and W. Wagner, "A new equation of state for carbon dioxide covering the fluid region from the triple-point temperature to 1100 K at pressures up to 800 MPa," *Journal of Physical and Chemical Reference Data*, vol. 25, no. 6, pp. 1509–1596, 1996.

[29] V. Vesovic, W. A. Wakeham, G. A. Olchowy, J. V. Sengers, J. T. R. Watson, and J. Millat, "The transport properties of carbon dioxide," *Journal of Physical and Chemical Reference Data*, vol. 19, no. 3, pp. 763–808, 1990.